International Journal of Fracture **66**: 45–70, 1994.

The peeling of flexible laminates

A.J. KINLOCH, C.C. LAU and J.G. WILLIAMS
Department of Mechanical Engineering, Imperial College of Science, Technology and Medicine, Exhibition Road, London SW7 2BX, UK

Received 19 July 1993; accepted in revised form 19 January 1994

Abstract. The present work has defined an adhesive fracture energy G_a for the peel testing of flexible laminates. The value of G_a characterises the fracture of the laminate and is considered to be a 'geometry-independent' parameter which reflects (i) the energy to break the interfacial bonding forces and (ii) the energy dissipated *locally* ahead of the peel front in the plastic or viscoelastic zone. We have shown that in order to determine this true adhesive fracture energy G_a that the following energy terms must be considered: (i) the stored strain-energy in the peeling arm, (ii) the energy dissipated during tensile deformation of the peeling arm, and (iii) the energy dissipated due to bending of the peeling arm. The analysis proposed yields quantitative expressions for these various energy dissipation terms and, in particular, considers the energy dissipated due to bending of the peeling arm. Another important feature of the analysis is the modelling of the region below the peel front as an elastic beam on an elastic foundation; such that the peeling arm does not act as a truly built-in beam and root rotation at the peel front is allowed. The analysis described in the present paper has been employed for four different laminates. The values of the local angle θ_0 at the peel front from the theoretical calculations have been shown to be in excellent agreement with the experimentally measured values; a small-scale peel test rig having been built so that the peel test, as a function of applied peel angle θ, thickness h of peeling arm and rate of test, could be observed and photographed using a stereo-optical microscope. The value of the adhesive fracture energy G_a (i.e. the 'fully corrected' value) for each laminate is indeed shown to be a 'material parameter'.

1. Introduction

The peel test is illustrated schematically in Fig. 1 and is one of the most frequently used test methods for assessing the failure of flexible laminates, such as those employed in the packaging and electronic industries. It has therefore been extensively studied [1-26] and a large amount of experimental and theoretical work exists on the effects of such parameters as the peel angle employed, the thickness of the materials, the degree of intrinsic adhesion acting between the materials, the effects of test rate and temperature, etc.

An aim of much of this work has been to identify a parameter which is a characteristic of the peeling of the laminate, independent of the exact details of the peel test geometry. Early work [2, 7] recognised that, for a given laminate of width b tested at a given rate and temperature, the applied peel angle θ would affect the value of the measured peel force P. Hence, expressions, based upon an energy-balance approach, were derived which attempted to account for the effect of peel angle. Also, it was recognised that tensile deformation of the

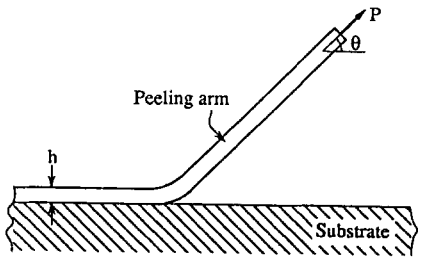

Fig. 1. The basic peel test.

peeling arm would affect the external work done and, further, could affect how much of the external work was actually available for debonding the laminate. Since tensile deformation of the arm may lead to:

(i) stored strain-energy in the peeling arm, and
(ii) plastic or viscoelastic energy dissipation in the peeling arm;

therefore, these effects were also taken into account, and in many cases these corrections are sufficient to yield values of the adhesive fracture energy which are independent of the exact details of the geometry of the peel test.

Also, previous work [3, 6] has clearly revealed that for most laminates the value of the adhesive fracture energy is a function of the rate and temperature of test. Since the value of the adhesive fracture energy will reflect not only the energy to break the interfacial bonding forces, but also the energy dissipated *locally* ahead of the peel front in the plastic or viscoelastic zone at the crack tip, this observation is to be expected [26].

Nevertheless, for many laminates the approaches outlined above have been found to be inadequate to yield a value of the adhesive fracture energy which represents a 'material parameter'; i.e. they do not result in a unique value for a given laminate which is independent of the exact details of the peel test geometry. This observation led Gent and Hamed [11, 13, 16] to suggest that an important aspect in many peel tests was the energy dissipated in plastic bending of the peeling arm. This aspect has subsequently been developed in some detail by Kim and Aravas and co-workers [19–22]. Attention [15, 24, 27, 28] has also been drawn to the effect that the mode of loading may have upon the value of the adhesive fracture energy. This effect arises from the ratio of mode I (i.e. tensile) to mode II (in-plane shear) loading varying as the peel angle θ is changed [24, 27]; and the possibility that changing this ratio might affect the value of the measured adhesive fracture energy.

The present work examines the peeling of flexible laminates and, in particular, considers the effects of plastic bending of the peeling arm. A major aim is to derive quantitative expressions for the energy dissipated by plastic deformation due to bending of the beam and thereby to correct the measured peel force for such energy losses. A novel aspect in solving this problem is to model the peel test as an elastic beam on an elastic foundation and consider the role of root rotation of the peel front. Thus, it is hoped that a true adhesive fracture energy G_a may be obtained which is independent of the geometry of the peel test. The validity of this modelling will be examined by conducting peel tests on the stage of a stereo-optical microscope so that the local angle θ_0 at the peel front can be experimentally measured and compared to the theoretically calculated values. Also, in order to validate the analysis proposed, the independence of the calculated value of G_a for a given laminate from such factors as the applied peel angle θ and thickness h of the peeling arm will also be explored.

2. Theoretical

2.1. Basic concepts

The adhesive fracture energy G_a may be derived from an energy-balance argument, such that

$$G_a = \frac{1}{b}\left(\frac{dU_{\text{ext}}}{da} - \frac{dU_s}{da} - \frac{dU_{dt}}{da} - \frac{dU_{db}}{da}\right), \tag{1}$$

where dU_{ext} is the external work, dU_s is the stored strain energy in the peeling arm, dU_{dt} is the energy dissipated during tensile deformation of the peeling arm, and dU_{db} is the energy dissipated during bending of the peeling arm near the peel front.

The value of G_a is considered to be a 'geometry-independent' parameter which characterises the fracture of the laminate. It reflects the energy to break the interfacial bonding forces and the energy dissipated *locally* ahead of the peel front in the plastic or viscoelastic zone at the crack tip.

Now considering a peeling arm of thickness h and width b which is peeling in a steady state under a constant load P at an applied peel angle of θ, as shown in Fig. 1, then

$$\begin{aligned} dU_{\text{ext}} &= Pda(1 + \varepsilon_a - \cos\,\theta), \\ d(U_s + U_{dt}) &= bhda \int_0^{\varepsilon_a} \sigma \cdot \mathrm{d}\varepsilon, \end{aligned} \tag{2}$$

where ε_a is the tensile strain in the peeling arm.

Therefore, if the peeling arm is considered to have an infinite tensile stiffness (i.e. $\varepsilon_a = 0$) and a zero bending stiffness, assumptions which are frequently made and which give a test which is equivalent to peeling away a material which behaves as a piece of 'infinitely-rigid string', then we obtain the simple equation:

$$G_a^{\infty E} = \frac{P}{b}(1 - \cos\,\theta). \tag{3}$$

If any tensile (i.e. stretching) deformation of the peeling arm is taken into account, but the bending of the peeling arm is assumed to be only elastic, then we obtain the equation:

$$G_a^{eb} = \frac{P}{b}(1 + \varepsilon_a - \cos\,\theta) - h \int_0^{\varepsilon_a} \sigma \cdot \mathrm{d}\varepsilon. \tag{4}$$

It should also be noted that the maximum elastic energy (per unit width per unit length), $G^e_{\max}$, which can be stored in the peeling arm for an elastic, non-work hardening material is given by

$$G^e_{\max} = \tfrac{1}{2}(\sigma\varepsilon_y h) = \tfrac{1}{2}(E\varepsilon_y^2 h), \tag{5}$$

where ε_y is the yield strain and E is the Young's modulus of the peeling arm (see Fig. 2 with $\alpha = 0$).

2.2. Local plastic bending

Now, if plastic or viscoelastic bending of the peeling arm occurs near the crack front, then the determination of G_a needs to take such energy losses into account. Thus, the value of G_a is given by

$$G_a = \frac{P}{b}(1 + \varepsilon_a - \cos\,\theta) - h \int_0^{\varepsilon_a} \sigma \cdot \mathrm{d}\varepsilon - G_{db}, \tag{6}$$

where $G_{db} = dU_{db}/b \cdot da$. From (4), an alternative representation of (6) is, therefore:

$$G_a = G_a^{eb} - G_{db}. \tag{7}$$

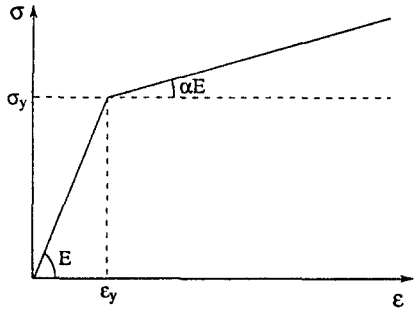

Fig. 2. Schematic of the bilinear, work-hardening representation for the stress versus strain curves.

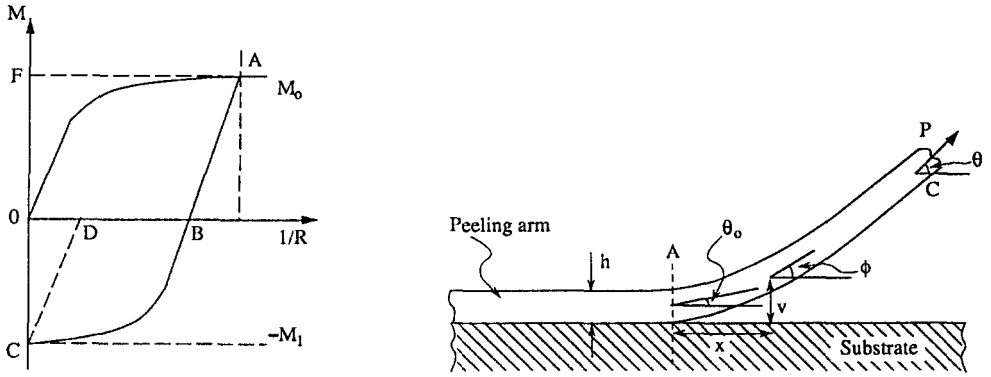

Fig. 3. Deformation of the peeling arm. (a) Deformation process undergone by the peeling arm. (b) Large-displacement beam-theory model of the peel test.

Obviously, the value of G_a^{eb} can be evaluated simply from (4), and it is the evaluation of G_{db} which is needed to enable the determination of G_a.

The deformation process is one of predominantly bending with large displacements. In the steady state the peeling arm is loaded rapidly up to some maximum moment at which crack propagation occurs and then *unloads* as the section moves backwards. In the plastic case there must be reverse bending to straighten the arm remote from the peel front. The deformation process is illustrated in Fig. 3 and it is clear that bending in the arm is unloading during the growth of the crack and goes from 'A', where $M = M_0$, down to 'C', where $M = -M_1$. At 'A', the slope of the arm at the peel front is θ_0 (see below); whilst at 'C' it is θ, the applied peel angle. There is some elastic energy stored in the arm at 'C', given by the area [COD], but this is lost in the sense that it is not available from the debonding process. The total energy loss in the loading and unloading cycle is the area [OABC] in Fig. 3a. Thus:

$$G_{db} = \frac{\text{Area[OABC]}}{b} = \frac{A_1}{b}. \tag{8}$$

The deformation process described above, and shown in Fig. 3a, may be modelled using large displacement beam theory which is best undertaken in terms of the slope ϕ at a point with coordinates x and v, as shown in Fig. 3b. The general scheme for modelling the local bending has been given previously [19–22] and the same scheme is followed here in Appendix A. Further, the elastic–plastic behaviour of the peeling arm has been modelled as a bilinear, work-hardening material, as shown in Fig. 2. This form of model provides a good fit for the

experimental stress versus strain curves for many polymers. Hence, the values of the Young's modulus E, plastic yield strain ε_y and work-hardening parameter α may be ascertained. From these models, the expressions described below may be derived for the different cases (see Appendix A).

The first case is when the bending of the peeling arm, during both the initial loading process (i.e. at the peel front) and the subsequent straightening and unloading process (i.e. which occurs in the now-debonded peel arm away from the peel front) only involves elastic deformation. Hence:

Case 1, which arises when $0 < k_0 < 1$, and we have:

$$\frac{G_{db}}{G^e_{\max}} = 0 \quad \text{and} \tag{9}$$

$$\frac{G_a^{\infty E}}{G^e_{\max}} = \frac{(1 - \cos\,\theta)}{[1 - \cos(\theta - \theta_0)]} \cdot \frac{k_0^2}{3}. \tag{10}$$

The second case is when the initial bending of the peeling arm involves plastic deformation but the unloading and straightening of the arm involves only elastic deformation. Hence:

Case 2, which arises when $1 < k_0 < 2(1 - \alpha)/(1 - 2\alpha)$ or $\alpha \geqslant 0.5$, and we have:

$$\frac{G_{db}}{G^e_{\max}} = (1 - \alpha)\left[\frac{k_0^2}{3} + \frac{2(1 - \alpha)^2}{3k_0} - 1\right], \quad \text{and} \tag{11}$$

$$\frac{G_a^{\infty E}}{G^e_{\max}} = \frac{(1 - \cos\,\theta)}{[1 - \cos(\theta - \theta_0)]} \cdot \frac{k_0^2}{3}. \tag{12}$$

The third case is when the loading and unloading of the peeling arm both involve plastic deformation. Hence:

Case 3, which arises when $k_0 > 2(1 - \alpha)/(1 - 2\alpha)$ and $\alpha < 0.5$, and we have:

$$\frac{G_{db}}{G^e_{\max}} = f_1(k_0), \quad \text{and} \tag{13}$$

$$\frac{G_a^{\infty E}}{G^e_{\max}} = \frac{(1 - \cos\,\theta)}{[1 - \cos(\theta - \theta_0)]} \cdot f_2(k_0), \tag{14}$$

where

$$f_1(k_0) = \tfrac{4}{3}\alpha(1 - \alpha)^2 k_0^2 + 2(1 - \alpha)^2(1 - 2\alpha)k_0 + \frac{2(1 - \alpha)}{3(1 - 2\alpha)k_0}[1 + 4(1 - \alpha)^3] - (1 - \alpha)[1 + 4(1 - \alpha)^2] \tag{15}$$

$$f_2(k_0) = \tfrac{1}{3}\alpha[1 + 4(1 - \alpha)^2]k_0^2 + 2(1 - \alpha)^2(1 - 2\alpha)k_0 + \frac{8}{3}\frac{(1 - \alpha)^4}{(1 - 2\alpha)k_0} - 4(1 - \alpha)^3. \tag{16}$$

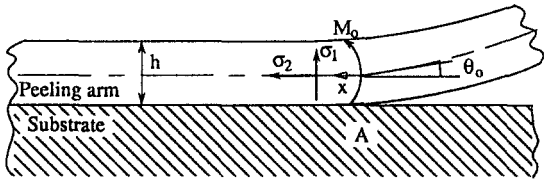

Fig. 4. Region below the peel front.

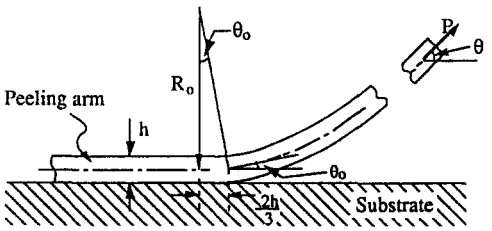

Fig. 5. Root rotation in the peel test.

The term k_0 is given by

$$k_0 = \frac{R_1}{R_0}, \tag{17}$$

where R_0 is the actual radius of curvature at the peel front and R_1 is the radius of curvature at the onset of plastic yielding and is given by

$$R_1 = \frac{h}{2\varepsilon_y}. \tag{18}$$

2.3. Root rotation at the peel front

Figure 4 shows the region below the peel front when the substrate layer is assumed to be adhered to a rigid plate such that the transverse strains are constrained to be zero. The deformation has been modelled as an elastic beam on an elastic foundation of thickness $\frac{1}{2}h$. This latter assumption has been explored by several authors [29, 30] and found to be accurate. The beam deformation may be analysed using:

$$\frac{\mathrm{d}^4 v}{\mathrm{d}x^4} = -\frac{w}{EI}, \tag{19}$$

where w is the distributed load per unit length on the beam and I is the moment of inertia. This may now be estimated from

$$w = \left[\frac{2v}{h}\right] Eb, \tag{20}$$

and, hence

$$\frac{\mathrm{d}^4 v}{\mathrm{d}x^4} = -\frac{24v}{h^4}. \tag{21}$$

For a bending moment M_0 applied at $x = 0$ and no direct loading with both v and $\mathrm{d}v/\mathrm{d}x \to 0$ at $x \to \infty$, this has the solution

$$\begin{aligned} &\frac{\mathrm{d}v}{\mathrm{d}x} = -\frac{12}{6^{1/4}} \cdot \frac{M_0}{Ebh^2} \cdot \mathrm{e}^{-6^{1/4}x/h} \cdot \cos^{6^{1/4}x/h} \quad \text{at } x = 0, \\ &\frac{\mathrm{d}v}{\mathrm{d}x} = -\theta_0 \quad \text{and} \quad \frac{12M_0}{Ebh^2} = \frac{h}{R_0}, \end{aligned} \tag{22}$$

we have

$$\theta_0 = \frac{h}{6^{1/4}R_0}. \tag{23}$$

More complete solutions including shear effects [29] have shown that the factor $1/6^{1/4}$ $(= 0.64)$ is better taken to have the value $\frac{2}{3}$. Hence, the fact that the beam does *not* act as a truly built-in beam is allowed for by extending the length of the beam by a distance $\frac{2}{3}h$, as shown in Fig. 5 where it may be seen that the slope of the beam is zero not at the peel front, but at a distance $\frac{2}{3}h$ ahead of the peel front, and $\theta_0 > 0°$. Thus, using (17) and (18), Eqn. (23) becomes

$$\theta_0 = \tfrac{1}{3}(4\varepsilon_y) \cdot k_0. \tag{24}$$

It is of interest to consider the effects of root rotation at the peel front. Obviously, if the value of $\theta_0 = 0°$, then the peel arm does act as a built-in beam and no root rotation occurs. In this case all the energy that is needed to fail the laminate has to be transmitted to the interfacial regions via bending of the arm of the laminate. If $\theta_0 > 0$ then the peel arm does not act as a built-in beam and root rotation at the peel front occurs. At the extreme then $\theta_0 = \theta$, which means that the material forming the peel arm has a zero bending modulus. This is equivalent to peeling away a material which behaves as 'string' and all the energy for peeling is transmitted directly to the interfacial regions, with none going via bending of the arm. More likely situations are when $0° < \theta_0 < \theta$, and in these cases some degree of root rotation occurs and the applied energy may be partitioned between that part which is transmitted via bending of the arm, and the remaining portion which is transmitted directly to the peeling process. Finally, it is of interest to note that the role of root rotation in peel tests has been previously mentioned by Kim and Kim [21], but they did not model this effect.

2.4. Evaluation of G_{db}

The contribution of plastic bending of the peel arm may now be determined via the evaluation of G_{db}. To determine the value of G_{db} the method used was firstly to deduce $G_a^{\infty E}$ from (3), G_a^{eb} from (4) and that of $G^e_{\max}$ using (5). Secondly, one has to decide whether the material behaviour falls under 'case 1', 'case 2' or 'case 3'; see (9) to (14). This is decided by determining the work-hardening parameter α from the shape of the stress versus strain curve for the material forming the peel arm and obtaining an initial estimate of k_0, using the equations for either 'case 2' or 'case 3', together with (24), and iterating to determine the values of k_0 and θ_0 which satisfy the pair of equations given for each case. The selection of the appropriate 'case' can then be made. For most polymeric materials, including those studied in the present investigation, 'case 3' represents the material behaviour. Hence, thirdly, one has to use (14) and (24) to iterate in order to determine the values of k_0 and θ_0 which satisfy both of these equations. A simple computer program was written to undertake this task and is listed in Appendix B. (It is written in 'C' language and needs a 'C' compiler to run the program.) Fourthly, the value of G_{db} may be determined using (13). Finally, the adhesive fracture energy G_a may now be calculated using (6).

Apart from examining the values of G_a for a given laminate to see whether they are indeed independent of experimental parameters such as peel angle and thickness of the peel arm, the value of the slope of the peel arm at the crack front provides a further cross-check on the accuracy of the analysis, since the values of θ_0 which are calculated as described above may be compared with values determined experimentally. To enable sound experimental values to be measured, a small-scale peel rig has been designed and built and the peel test has been observed using a stereo-optical microscope, and this is described below.

3. Experimental

3.1. The materials

The various flexible laminates which were examined were:

(i) A film of polyethylene (PE1) adhered to an aluminium foil, and this was the main flexible laminate which was employed for the present studies. The polyethylene was processed by extrusion coating directly onto the aluminium foil, which was about 6 μm thick. A series of such laminates were prepared where the thickness of the polyethylene (PE1) film was varied from about 30 to 250 μm. These are termed PE1/Al-foil laminates. To undertake the peel test, the aluminium foil was bonded to a rigid support block of poly(methyl methacrylate) (PMMA) and the polyethylene film was peeled away from the foil bonded to the PMMA block (i.e. the aluminium foil bonded to the PMMA block is termed the 'substrate' in Fig. 1, and the peeling arm is the PE1 film).

(ii) A film of polyethylene (PE2) adhered to an aluminium foil. The polyethylene was laminated onto the aluminium foil, which was about 6 μm thick. These are termed PE2/Al-foil laminates. This polyethylene (PE2) film differed from the previous one (i.e. PE1) with respect to molecular-weight distribution and degree of orientation. These different physical properties lead to different mechanical properties of the two polyethylene films. The film of PE2 formed the peeling arm, and during the peel tests was debonded from the aluminium foil bonded to the PMMA support block (i.e. from the 'substrate').

(iii) A polyethylene (PE1) film adhered to a poly(ethylene terephthalate) (PET) film. The polyethylene was processed by extrusion coating onto the PET film, but a tie-layer adhesive was also simultaneously melt-extruded between the PE1 and PET films to increase the adhesion. The tie-layer adhesive (T1) was a modified polyethylene. The PE1 and PET films were about 20 and 12 μm thick, respectively, and the tie-layer adhesive (T1) was about 10 μm thick. These are termed PET/T1/PE1 laminates. To undertake the peel test for these laminates, the PET film was peeled away from the PE1 which was bonded to the PMMA support block (i.e. the PE1 film bonded to the PMMA block is termed the 'substrate' in Fig. 1).

(iv) A polyethylene (PE1) film adhered to a poly(ethylene terephthalate) (PET) film. The polyethylene was processed by extrusion coating onto the PET film, but a tie-layer adhesive was also simultaneously melt-extruded between the PE1 and PET films to increase the adhesion. A different tie-layer adhesive (T2) was employed, but again was a modified polyethylene. The PE1 and PET films were about 20 and 12 μm thick, respectively, and the tie-layer adhesive (T2) was about 10 μm thick. These are termed PET/T2/PE1 laminates. Similarly, to undertake the peel test for these laminates, the PET film formed the peeling arm which was peeled away from the PE1 bonded to the PMMA support block (termed the 'substrate' in Fig. 1).

3.2. The peel test

The peel test employed in the current studies is shown in Fig. 6. A linear-bearing trolley was used to maintain a constant peel angle θ; and the peel angle was determined by the angle of the PMMA support block. Now, for the PE1/Al-foil and PE2/Al-foil laminates, the polyethylene film was peeled away from the aluminium foil, which was firmly adhered to the rigid support block of PMMA. These two laminates being different with respect to the type of polyethylene used in their manufacture. For the PET/T1/PEI and PET/T2/PE1 laminates, the PET film

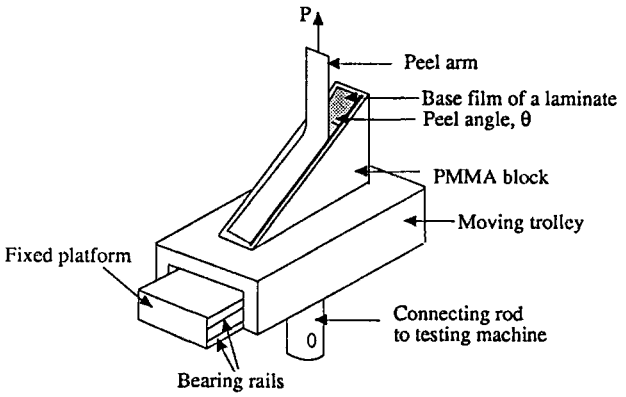

Fig. 6. The peel rig used for the constant angle peel tests.

was peeled away from the PE1 film, which was firmly adhered to the rigid support block of PMMA. These two laminates being different with respect to the type of tie-layer adhesive which was employed in their manufacture.

The peel angle was changed from 30° to 180°, by using different support blocks of PMMA, and the test was conducted at a constant rate of displacement, which was varied from 1 mm/min to 100 mm/min. Whilst some of the peel tests were conducted using a standard tensile testing machine (an 'Instron Model 1185'), many of the tests were undertaken using a small-scale peel test rig made specifically for the current research. This rig enabled the peel test to be conducted on the stage of a stereo-optical microscope so that micrographs and video film could be taken of the peel front for the various laminates examined at the different peel angles and test rates. During the peel tests, the load P required to debond the laminate was measured as a function of time, and the velocity with which the peel front moved was also measured. From measuring the thickness and width of the peeling arm, the stress in the arm could be determined and hence, from the stress versus strain curve (see below), the strain ε in the arm during steady-state peeling could be readily ascertained.

The PE1/Al-foil, PE2/Al-foil and PET/T2/PE1 laminates all failed in a stable manner. Namely, the peel front propagated steadily through the laminate and the peel load P which for the peeling process was virtually constant in value. The locus of failure of the laminates was apparently interfacial from a visual assessment. However, for the PET/T1/PE1 laminate the crack only propagated in a stable manner at rates of test below about 10 mm/min. At higher rates of test the peel front propagated unstably in a 'stick/slip' manner, with maximum and minimum values of the peel force being recorded. In the present work the maximum value of the peel force P was used for the calculation of the adhesive fracture energy. The reason for the 'stick/slip' crack growth in the PET/T1/PE1 laminates at the higher testing rates was considered possibly to be due to a change in the locus of failure as the crack propagated through the laminate. This type of behaviour has been previously recorded [31] for polyimide/acrylic-adhesive/copper foil laminates, and is discussed for the present laminates in detail elsewhere [32].

3.3. Tensile tests

The analysis of the peel test described above requires a knowledge of the tensile stress versus strain properties of the material which form the peeling arm of the peel test. These data were

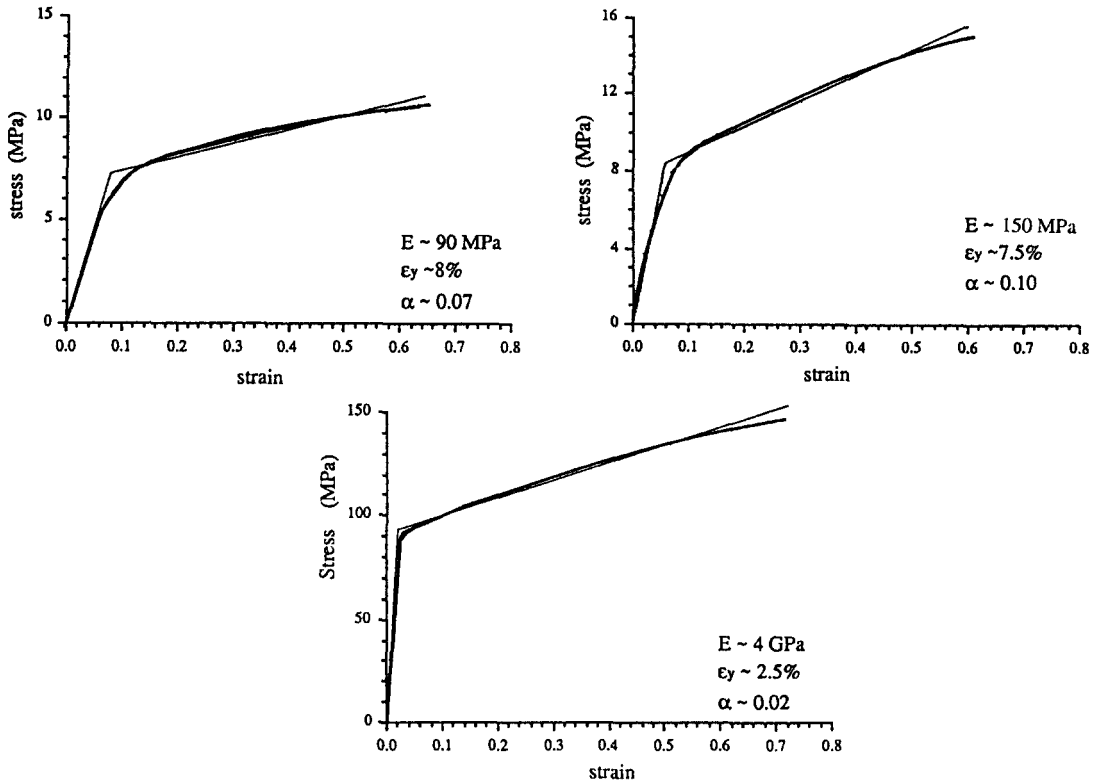

Fig. 7. Uniaxial tensile stress versus strain properties of the peeling arm materials (rate of test = 10 mm/min). The bilinear, work-hardening representations for the stress versus strain curves are also shown and the values of tensile modulus E yield strain ε_y and work-hardening parameter α from the representation are given. (a) Polyethylene (PE1). (b) Polyethylene (PE2). (c) Poly(ethylene terephthalate) (PET).

obtained by cutting dumb-bell shaped specimens from the materials which formed the peeling arms and testing the specimens in uniaxial tension at a constant rate of displacement. The rate of test was varied from 1 mm/min to 100 mm/min. Typical stress versus strain curves for the PE1, PE2 and PET film materials are shown in Fig. 7, together with the bilinear, work-hardening representation of the stress versus strain behaviour. As may be seen, this representation provides a good model for the stress versus strain properties of the material forming the arm in the peel test. The complete and detailed properties of all the materials examined at the various rates of test are reported elsewhere [32].

4. Results and discussion

4.1. Introduction

Experiments were conducted as described previously in Section 3.2 and the peel load P was measured as a function of peel angle θ for the different laminates. The peel test was also observed using the stereo-optical microscope and photographs were taken of the peel front. Examples of such micrographs are shown in Fig. 8.

As may be seen clearly from the micrographs, the first point of interest is that local angle θ_0 at the peel front does not equal zero. Thus, the peeling arm does not act as a built-in beam. Secondly, the value of θ_0 is lower than that of the applied peel angle θ. Thus, further, the

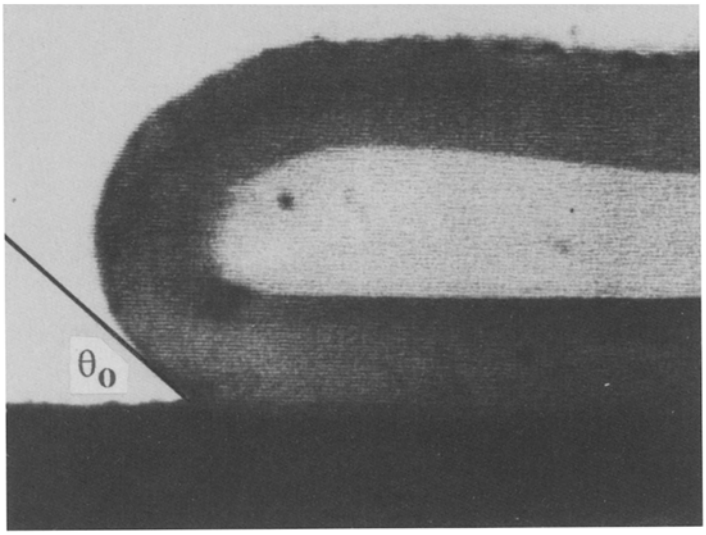

(a)

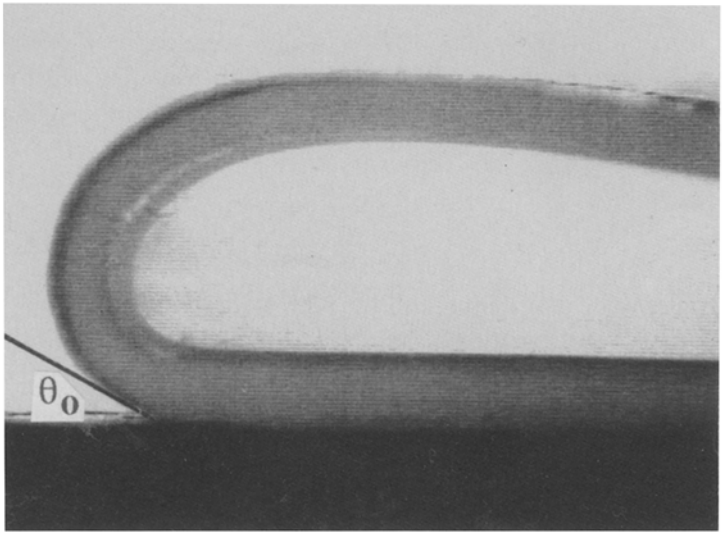

(b)

Fig. 8. Optical micrographs of the peel front. (a) PE1/Al-foil laminate; $\theta = 180°$; $h = 75$ μm; rate of test = 1 mm/min. (Peeling from left to right; taken at $\times 200$ magnification.) (b) PE1/Al-foil laminate; $\theta = 180°$; $h \simeq 165$ μm; rate of test = 1 mm/min. (Peeling from left to right; taken at $\times 100$ magnification.)

peeling arm does not act as a 'string' possessing a zero bending stiffness. Indeed, the value of θ_0 being greater than zero but less than θ clearly reveals that some of the energy for the debonding process is delivered by bending and that the rest is directly transmitted. It is this dual nature of the energy transmission which is, of course, modelled by the root rotation scheme which was discussed in Section 2.3. Further, the value of the local angle θ_0 must be quantitatively ascertained, together with the type of deformation which the peeling arm

Table 1. Results for the PE1/Al-foil laminates

Peel angle (°)	$G_a^{\infty E}$ (J/m^2)	θ_0 (theory) (°)	θ_0(expt.) (°)	G_a (J/m^2)
60	155	26.3	20 to 30	140
90	198	35.0	38 to 42	136
120	225	42.6	45 to 50	131
150	250	49.0	48 to 55	125

Notes: $\varepsilon_y = 8.9\%$; $E = 80$ MPa; $\alpha = 0.07$; $h = 35\ \mu m$. $G^e_{\max}$ =11.1 J/m^2 from (5); $G_a^{\infty E}$ from (3); θ_0 (theory) from (24); G_a from (6).

undergoes in the peel test, if accurate values of the energy dissipated during bending of the peeling arm near the peel front are to be determined. Obviously, once this energy loss G_{db} has been ascertained, the evaluation of the adhesive fracture energy G_a is straightforward via (6).

4.2. Effect of peel angle θ

As explained in Section 2.4, the values of E, ε_y and α were deduced from the stress versus strain curve of the material and an initial estimate of k_0 was obtained by iteration, using the computer program given in Appendix B. In the present work, the values of α and k_0 so determined were always such that:

$$k_0 > \frac{2(1-\alpha)}{(1-2\alpha)} \quad \text{and} \quad \alpha < 0.5. \tag{25}$$

Hence, the deformation of the peeling arm for both loading and unloading involves plastic deformation, i.e. 'case 3' deformation is appropriate to the current peel tests. Therefore, (14) and (24) were iterated, again using the computer program given in Appendix B, to obtain the values of k_0 and θ_0. Next, the value of G_{db} was deduced using (13), and finally that of G_a using (6). The results for the four different laminates are shown in Tables 1 to 4. The rate of test was 5 mm/min.

There are several noteworthy features of these results. Firstly, the values of the local angle θ_0 at the peel front calculated as described above are in very good agreement with the values determined from the experimental observations using the small-scale peel rig mounted on the stage of the stereo-optical microscope. This is further illustrated in Fig. 9 where the experimental values, determined from micrographs such as those shown in Fig. 8 are compared with the theoretically calculated values. The very good agreement between the experimental and theoretical values obviously supports the model proposed in Section 2. Secondly, the values of θ_0 are such that $0 < \theta_0 < \theta$, with the implications which were noted above. Thirdly, values of $G_a^{\infty E}$, which are deduced from (3) are, for any given laminate, clearly very dependent upon the peel angle used. (It will be recalled that this equation is for the case where the peeling arm is considered to have an infinite tensile stiffness and a zero bending stiffness; i.e. it behaves as a piece of 'infinitely-rigid string'. Also, note that in certain circumstances (e.g. in Table 2 for $\theta = 45°$) the value of $G_a^{\infty E}$ may be lower in value than G_a; this arises

Table 2. Results for the PE2/Al-foil laminates

Peel angle (°)	$G_a^{\infty E}$ (J/m^2)	θ_0 (theory) (°)	θ_0(expt.) (°)	G_a (J/m^2)
45	183	20.4	24 to 30	236
90	333	34.5	40 to 47	228
120	375	41.7	48 to 58	218
135	412	46.1	50 to 60	223
150	467	51.7	55 to 62	236

Notes: $\varepsilon_y = 7.8\%$; $E = 140$ MPa; $\alpha = 0.1$; $h = 35\ \mu m$. $G^e_{\max} = 14.9$ J/m^2 from (5); $G_a^{\infty E}$ from (3); θ_0 (theory) from (24); G_a from (6).

Table 3. Results for the PET/T1/PE1 laminates

Peel angle (°)	$G_a^{\infty E}$ (J/m^2)	θ_0 (theory) (°)	θ_0(expt.) (°)	G_a (J/m^2)
30	100	7.6	5 to 8	61.6
60	108	9.4	7 to 12	42.0
90	125	11.1	9 to 13	37.8
120	184	14.8	13 to 19	46.5
150	232	19.6	15 to 20	45.7

Notes: $\varepsilon_y = 2.4\%$; $E = 3800$ MPa; $\alpha = 0.03$; $h = 12\ \mu m$. $G^e_{\max} = 11.0$ J/m^2 from (5); $G_a^{\infty E}$ from (3); θ_0 (theory) from (24); G_a from (6).

Table 4. Results for the PET/T2/PE1 laminates

Peel angle (°)	$G_a^{\infty E}$ (J/m^2)	θ_0 (theory) (°)	θ_0(expt.) (°)	G_a (J/m^2)
30	44.2	5.3	5 to 10	24.6
60	80.0	8.0	8 to 12	29.7
90	78.0	8.5	8 to 13	22.8
120	90.0	9.6	9 to 14	21.3
150	119.0	11.8	10 to 15	22.0

Notes: $\varepsilon_y = 2.4\%$; $E = 3800$ MPa; $\alpha = 0.03$; $h = 12\ \mu m$. $G^e_{\max} = 11.0$ J/m^2 from (5); $G_a^{\infty E}$ from (3); θ_0 (theory) from (24); G_a from (6).

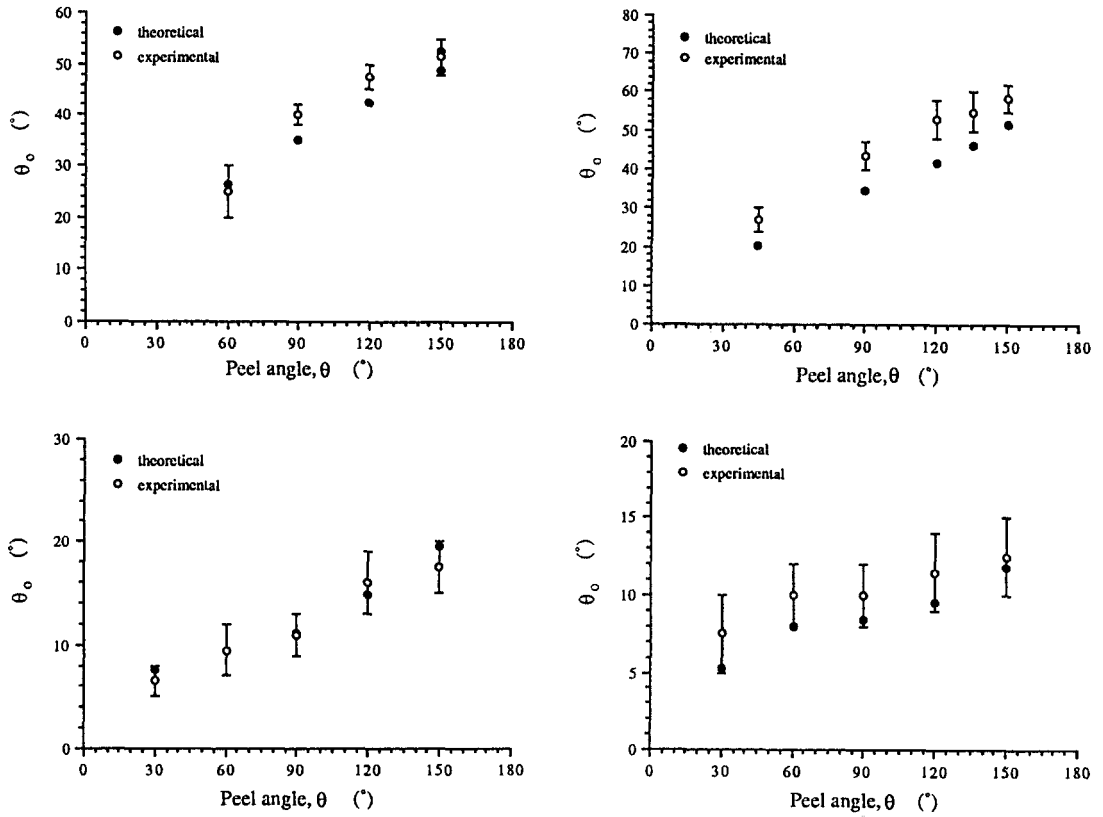

Fig. 9. Comparison of the theoretical and experimentally measured values of θ_0 as a function of the applied peel angle θ. (a) PE1/A1-foil laminates; $h = 35$ μm and rate of test = 5 mm/min. (b) PE2/A1-foil laminates; $h = 35$ μm and rate of test = 5 mm/min. (c) PET/T1/PE1 laminates; $h = 12$ μm and rate of test = 5 mm/min. (d) PET/T2/PE1 laminates; $h = 12$ μm and rate of test = 5 mm/min.

from the ε_a term in (6) being more significant than the values of the last two terms in this equation for some peel tests.)

Fourthly, however, as discussed earlier, to deduce the value of the true adhesive fracture energy G_a corrections are needed for:

(i) the stored strain energy in the peeling arm,

(ii) the energy dissipated during tensile deformation of the peeling arm, and

(iii) the energy dissipated due to bending of the peeling arm.

When these three correction terms are taken into account the values of the corresponding adhesive fracture energy G_a are indeed not significantly dependent upon the peel angle θ. This conclusion is reinforced by the mean values of G_a which are given in Table 5 for each of the laminates where, as may be seen, the associated scatter is very low. Now, the values of G_a reflect both (i) the energy to rupture the interfacial bonding forces, and (ii) the energy dissipated locally ahead of the peel front in the plastic or viscoelastic zone at the crack tip. The differences in the values of G_a for the two different laminates based upon polyethylene directly adhered to aluminium foil most probably reflect the different mechanical properties of the two polyethylenes, which differ in molecular-weight distribution and degree of crystallinity. In the case of the two poly(ethylene terephthalate) based laminates, the reason for the different

Table 5. Mean values of the adhesive fracture energy G_a for the laminates

Laminate	Adhesive fracture energy, G_a (J/m^2)	Coefficient of variation (%)
PE1/Al-foil	133±6	4.2
PE2/Al-foil	228±7	3.1
PET/T1/PE1	46.7±8.1	17.3
PET/T2/PE1	24.1±3.0	12.4

Note: mean ± one standard deviation is shown.

values of G_a is the use of different modified-polyethylene tie-layer adhesives (denoted by T1 and T2); the effect of changing the type of tie-layer adhesive being clearly demonstrated by the difference in the respective G_a values.

Finally, if only the first two of the above three correction terms stated above are considered, then the corresponding term so calculated is G_a^{eb} (see (4)). For the two laminates with the polyethylene peeling arms (i.e. see Tables 1 and 2) the values of G_a^{eb} and $G_a^{\infty E}$ were similar in value; with G_a^{eb} being somewhat higher than $G_a^{\infty E}$ at low peel angles, but G_a^{eb} and $G_a^{\infty E}$ being approximately equal in value at larger peel angles. For the two laminates with the poly (ethylene terephthlate) peeling arms (i.e. see Tables 3 and 4) the values of G_a^{eb} and $G_a^{\infty E}$ were always very similar in value. The main point is, of course, that the value of G_a^{eb} does not provide a constant, unique value, which is independent of peel angle θ for a given laminate. It is obviously of vital importance to take account of the third correction term, which allows for the energy dissipated due to bending of the peeling arm, in order to deduce a constant value, namely G_a.

4.3. Effect of thickness, h, of peeling arm

The effect of the thickness, h, of the peeling arm was investigated for the PE1/Al-foil laminates by using a peel angle θ of 180° and the thickness h of the polyethylene film was changed from 30 μm to 215 μm. The rate of test was kept constant for a given series of peel tests which employed the various thicknesses of polyethylene. The rate of test used was either 1, 10 or 50 mm/min. Typical results for the PE1/Al-foil laminates tested at 1 mm/min using a fixed peel angle θ of 180° are shown in Table 6. The values of the local angle θ_0 at the peel front were calculated as described above and were again in good agreement with the experimentally measured values. Also, for any given rate of test, the values of G_a were not significantly dependent upon the thickness h of the film. Indeed, for the results shown in Table 6, the value of G_a is 66.7±3.8 J/m^2; which gives a coefficient of variation for the mean value of G_a of only ±5.7 percent.

4.4. Effect of mode-mix

It is noteworthy that from the results shown in Tables 1 to 6 that there appears to be no need to invoke the proposition that the ratio of mode I : mode II loading (i.e. tensile opening to in-plane shear loading) varies as the applied peel angle θ or thickness h of the peeling arm is changed. A mixed-mode analysis [27, 32] gives the simple peel test (see Fig. 1), for $\varepsilon = 0$, as

Table 6. Results for the PE1/Al-foil laminates with various thicknesses h of PE1 (the peeling arm)

Thickness h (μm)	$G_a^{\infty E}$ (J/m^2)	θ_0 (theory) (°)	θ_0(expt.) (°)	G_a (J/m^2)
30	195	59.5	54 to 66	69.8
45	205	50.0	41 to 49	62.3
60	240	46.0	38 to 46	69.3
75	260	43.4	38 to 45	71.5
105	260	36.1	24 to 32	67.3
135	225	29.1	22 to 28	59.5
165	240	27.1	22 to 28	65.4
215	220	21.9	17 to 21	68.2

Notes: $\varepsilon_y = 9.4\%$; $E = 70$ MPa; $\alpha = 0.055$; rate of test 1 mm/min. G^e_{max} =0.31 J/m^2 per micron from (5); $G_a^{\infty E}$ from (3); θ_0 (theory) from (24); G_a from (6).

being pure mode I when $\theta \rightarrow 0°$, and pure mode II when $\theta = 180°$. However, obviously, one major reason that a mixed-mode analysis is not needed is that the local angle θ_0 at the peel front never actually experiences this extreme range of values used for the applied peel angle θ. For example, for the PE1/Al-foil laminates, when $\theta = 180°$ the value of θ_0 is about 60° for relatively thin peeling arms and only about 20° for relatively thick peeling arms, see Table 6. Also, whilst the applied peel angle θ may be varied from 60° to 150°, the local angle θ_0 may only change from about 25° to 50° for the PE1/Al-foil laminates, see Table 1; or from 10° to 12° for the PET/T2/PE1 laminates, see Table 4. Hence, the actual range of mode I : II ratios experienced by the crack tip regions during the peel test is relatively very limited. Another reason that a mixed-mode analysis is not needed may arise from the frequent observation that, if the pure mode I and mode II values of G_a were indeed deduced by some method, it might well be found that $G_{Ia} \cong G_{IIa}$. Hence, again, no significant effect of the ratio of mode I : mode II loading would be expected on the measured value of G_a.

4.5. Effect of test rate

The effect of the rate of test was studied from the series of tests reported above in Section 4.3. However, it was also studied by conducting peel tests at an applied peel angle θ of 180° over a wide range of applied rates for a constant thickness h of the polyethylene film of 35 μm.

The calculated values of G_a for the PE1/Al-foil laminates from the various tests which examined the effect of peel angle, θ, thickness, h, and rate of test are plotted against the peel front or crack velocity in Fig. 10, where the peel front velocity is given by the rate of test divided by $(1 - \cos\theta + \varepsilon_a)$. The data in Fig. 10 show that the value of G_a is dependent upon the crack velocity, where the crack velocity has been varied over about two and half decades of rate. This is not unexpected, since the value of G_a does indeed reflect the plastic or viscoelastic energy dissipated locally in the zone ahead of the crack, and this energy loss will be rate and temperature dependent. It should be noted that this dependence of G_a upon rate of crack velocity does, in theory, raise a problem when comparing the values of G_a. Namely, for

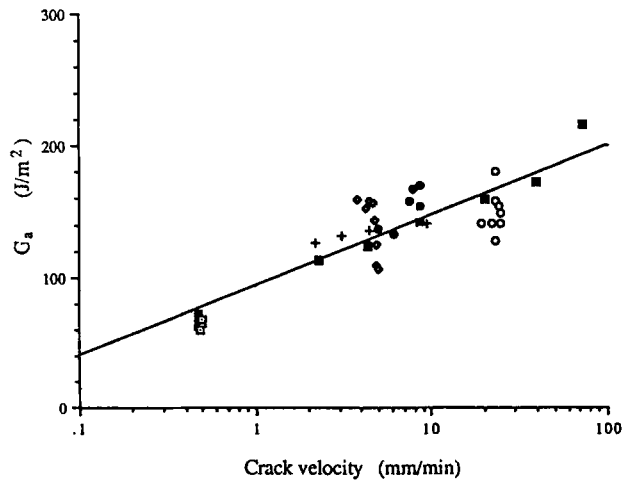

Fig. 10. The adhesive fracture energy G_a versus the peel front velocity for the PE1/Al-foil laminates as a function of peel angle (θ), thickness (h) of PE1 and rate of test. + 5 mm/min and $h = 35$ μm at various peel angles. • 10mm/min and $h = 35$ μm at various peel angles. ⊡ 180° peel angle and 1 mm/min at various h values. ◊ 180° peel angle and 10 mm/min at various h values. o 180° peel angle and 50 mm/min at various h values. ■ 180° peel angle and $h = 35$ μm at various rates of test.

a given series of tests undertaken at a given rate of test, the actual peel front velocity will be somewhat different for tests conducted at different applied peel angles θ and where the strain ε_a in the peeling arm is not constant. However, in the present experiments, the actual variation in the crack velocity for any series of tests conducted at a given rate of test was relatively low compared to the two and half decades of velocity shown in Fig. 10; the variation typically being of the order of $\pm 2\%$ to $\pm 45\%$ of the average peel front velocity. From the experimental results shown in Fig. 10, this degree of variation in the crack velocity would not be expected to significantly affect the value of G_a.

The observation that the value of G_a decreases as the crack velocity decreases is in agreement with previous work [6, 8, 9] where it was found that the adhesive fracture energy G_a for a styrene-butadiene rubber adhering to various polymeric substrates decreased as the peeling velocity was decreased. Indeed, at very low velocities, the value of G_a approached that of the thermodynamic work of adhesion W_a; where W_a is a direct measure of the molecular bonding forces acting across the interface and is of the order of 0.05 J/m^2 in value for an interface where secondary, van der Walas forces are acting. However, more work is obviously needed to determine whether the value of G_a for the present laminates would decrease to such very low values, of the order of W_a, as the crack velocity is further reduced.

5. Conclusions

The present work has analysed the peeling of flexible laminates using an energy-balance approach. We have defined an adhesive fracture energy G_a which is considered to be a 'geometry-independent' parameter, and the value of G_a characterises the fracture of the laminate. It reflects the energy to break the interfacial bonding forces and the energy dissipated *locally* ahead of the peel front in the plastic or viscoelastic zone at the crack tip.

We have shown that in order to determine this true adhesive fracture energy G_a that the following energy terms must be considered:

(i) the stored strain energy in the peeling arm,

(ii) the energy dissipated during tensile deformation of the peeling arm, and

(iii) the energy dissipated due to bending of the peeling arm.

The analysis proposed gives expressions for these various energy terms and, in particular, considers the energy dissipated due to bending of the peeling arm. For the energy dissipated due to bending of the peeling arm, three different cases have been identified. The first case is when the bending of the peeling arm, during both the initial loading process (i.e. at the peel front) and the subsequent straightening and unloading process (i.e. which occurs in the now-debonded peel arm away from the peel front) only involves elastic deformation. The second case is when the initial bending of the peeling arm involves plastic deformation but the unloading and straightening of the arm involves only elastic deformation. The third case is when the loading and unloading of the peeling arm both involve plastic deformation. This last case is shown to be the operative one for the laminates studied in the present work. For these three cases quantitative expressions for the energy dissipated due to bending of the peeling arm have been derived, using a bilinear work-hardening representation for the stress versus strain behaviour of the material which forms the peeling arm.

Another important feature of the analysis is the modelling of the region below the peel front as an elastic beam on an elastic foundation, such that the peeling arm does not act as a truly built-in beam and root rotation at the peel front is allowed. If the peeling arm deforms as a beam, but no root rotation is allowed, then the local angle at the peel front θ_0 has a value of zero and the peel arm does act as a built-in beam. In this case all the energy that is needed to fail the laminate has to be transmitted to the interfacial regions via bending of the arm of the laminate. If $\theta_0 > 0°$ then the peel arm does not act as a built-in beam and root rotation at the peel front occurs. At the extreme then $\theta_0 = \theta$, which means that the material forming the peel arm has a zero bending modulus. This is equivalent to peeling away a material which behaves as 'string', and all the energy for peeling is transmitted directly to the interfacial regions, with none going via bending of the arm. More likely situations, such as those in the present work, are when $0° < \theta_0 < \theta$. In these cases some degree of root rotation occurs and the applied energy may be partitioned between that part which is transmitted via bending of the arm, and the remaining portion which is transmitted directly to the peeling process. Thus, treating the peeling arm as a beam and allowing root rotation to occur at the peel front are both essential features in analysing the peel test.

The analysis described in the present paper has been employed for four different laminates. The values of θ_0 from the theoretical calculations have been shown to be in excellent agreement with the experimentally measured values; a small-scale peel rig having been built so that the peel test, as a function of applied peel angle θ, thickness h, of peeling arm, and rate of test, could be observed and photographed using a stereo-optical microscope. The value of the adhesive fracture energy G_a (i.e. the 'fully corrected' value) is indeed shown to be a 'material parameter'. The value of G_a for any laminate is independent of the test geometry (i.e. applied peel angle θ and thickness h of the peeling arm). However, for the polyethylene-aluminium foil (i.e. the PE1/Al-foil) laminates the value of G_a has been determined over a wide range of crack velocities (i.e. about two and half decades), and G_a has been found to be a function of the velocity with which the peel front propagates through the laminate.

Appendix A

The general scheme for modelling the local bending has been given previously [19–22] and we shall use the same nomenclature here. The deformation processes shown in Fig. 3(a) may be modelled using large displacement beam theory; which is best undertaken in terms of the slope ϕ at a point with coordinates x and v as shown in Fig. 3(b). If the load point coordinates are v_0 and x_0 the moment at any point is

$$M = P[(x_0 - x)\ \sin\ \theta - (v_0 - v)\ \cos\ \theta] \tag{A.1}$$

and

$$\frac{\mathrm{d}M}{\mathrm{d}\phi} = -P\left[\frac{\mathrm{d}x}{\mathrm{d}\phi}\ \sin\ \theta - \frac{\mathrm{d}v}{\mathrm{d}\phi}\ \cos\ \theta\right]. \tag{A.2}$$

For a beam length of s we have

$$\frac{\mathrm{d}v}{\mathrm{d}s} = \sin\ \phi, \quad \frac{\mathrm{d}x}{\mathrm{d}s} = \cos\ \phi \quad \text{and} \quad \frac{\mathrm{d}\phi}{\mathrm{d}s} = \frac{1}{R}, \tag{A.3}$$

where R is the local radius of curvature and hence

$$\frac{\mathrm{d}x}{\mathrm{d}\phi} = R\ \cos\ \phi \quad \text{and} \quad \frac{\mathrm{d}x}{\mathrm{d}\phi} = R\ \sin\ \phi, \tag{A.4}$$

giving

$$\frac{\mathrm{d}M}{\mathrm{d}\phi} = -PR\ \sin[\theta - \phi], \tag{A.5}$$

$$\therefore \int_{-M_1}^{+M_0} \frac{\mathrm{d}M}{R} = -P\int_{\theta}^{\theta_0} \sin(\theta - \phi)\ \mathrm{d}\phi. \tag{A.6}$$

Now in the unloading process in Fig. 3(a), we have:

$$A_2 = \int_{-M_1}^{+M_0} \frac{\mathrm{d}M}{R} = \text{Area[OFABC]} = P[1 - \cos(\theta - \theta_0)]. \tag{A.7}$$

Now the area A_1 is given by [OABC], and $A_1/b = G_{db}$ (see (8)). Thus, it is noteworthy that if $\theta_0 = 0$ and the strains are small, then $A_2 = bG_a^{\infty E}$ (i.e. compare (A.7) and (3)) and so (from (7))

$$G_a = \frac{A_2 - A_1}{b}, \tag{A.8}$$

i.e. G_a is given by the area [OFAD] in Fig. 3(a).

However, when $\theta_0 \neq 0$ not all the energy goes via bending and hence the determination of θ_0 is important in determining G_a. The areas A_1 and A_2 have, therefore, to be deduced and we can model the material by:

For $\quad \varepsilon/\varepsilon_y < 1, \quad \sigma = E\varepsilon;$ and

for $\quad \varepsilon/\varepsilon_y > 1, \quad \sigma = E\varepsilon_y f(\varepsilon/\varepsilon_y).$

(Note, that for a bilinear work-hardening material we have

$$f = (1 - \alpha) + \alpha \left(\frac{\varepsilon}{\varepsilon_y} \right) \tag{A.9}$$

and α is defined in Fig. 2.)

Now the moment at any section is given by

$$M = 2b \int_0^{h/2} \sigma \cdot y \cdot \mathrm{d}y, \tag{A.10}$$

where y is the distance from the neutral axis. On loading, the strain at any section is

$$\varepsilon = \frac{y}{R}. \tag{A.11}$$

It is convenient to scale these results using the collapse moment for a non-work hardening material (i.e. for a bilinear model, then $\alpha = 0$)

$$M_p = \tfrac{1}{4}(bh^2 E \varepsilon_y), \tag{A.12}$$

and the radius at first yields

$$R_1 = \frac{h}{2\varepsilon_y}. \tag{A.13}$$

We may now write the variables

$$m = \frac{M}{M_p}, \quad k = \frac{R_1}{R} \quad \text{and} \quad \zeta = \frac{2y}{h}, \tag{A.14}$$

and

$$m = 2 \int_0^1 \left(\frac{\sigma}{E\varepsilon_y} \right) \zeta \cdot \mathrm{d}\zeta, \tag{A.15}$$

and

$$\varepsilon = \varepsilon_y k \zeta. \tag{A.16}$$

We may now define four regions of behaviour in the m–k relationship:

(i) Elastic loading:

In this region

$$\begin{aligned} &\frac{\varepsilon}{\varepsilon_y} < 1 \quad \text{for} \quad \zeta = 1, \quad \text{i.e. } 0 < k < 1, \\ &\therefore \frac{\sigma}{E\varepsilon_y} = k\zeta \quad \text{and} \quad m_i = 2k \int_0^1 \zeta^2 \, \mathrm{d}\zeta = \tfrac{2}{3}k, \quad 0 < k < 1. \end{aligned} \tag{A.17}$$

(ii) Elastic–plastic loading:

In this region

$$\begin{aligned}
&\frac{\sigma}{E\varepsilon_y} = k\zeta, \quad 0 < \zeta < \frac{1}{k}\left(\varepsilon = \varepsilon_y,\ \zeta = \frac{1}{k}\right),\\
&\frac{\sigma}{E\varepsilon_y} = f(k\zeta), \quad \frac{1}{k} < \zeta < 1,\\
&\therefore m = 2k\int_0^{1/k} \zeta^2\,\mathrm{d}\zeta + 2\int_{1/k}^{1} f(k\zeta)\cdot\zeta\,\mathrm{d}\zeta,\\
&\text{i.e.}\quad m_{ii} = \frac{2}{3k^2} + 2\int_{1/k}^{1} f(k\zeta)\cdot\zeta\,\mathrm{d}\zeta.
\end{aligned} \tag{A.18}$$

(iii) Elastic unloading:

In this region

$$\varepsilon = y\left(\frac{1}{R_0} - \frac{1}{R}\right), \tag{A.19}$$

where R_0 is the radius at the maximum moment, hence

$$\varepsilon = \varepsilon_y(k_0 - k)\zeta, \tag{A.20}$$

and, if we assume that $m = m_0$ at $k = k_0$, then

$$m_{iii} = m_0 - 2\int_0^1 (k_0 - k)\zeta^2\,\mathrm{d}\zeta = m_0 - \tfrac{2}{3}(k_0 - k). \tag{A.21}$$

The unloading remains elastic until yielding is induced at the outer fibres ($\zeta = 1$). This condition is when

$$\begin{aligned}
&E\varepsilon_y f(k_0) - E\varepsilon_y(k_0 - k_1) = -E\varepsilon_y f(k_0),\\
&\text{i.e.}\quad k_1 = k_0 - 2f(k_0).
\end{aligned} \tag{A.22}$$

(iv) Reverse elastic–plastic unloading:

In this region, the interface at which reverse yielding first occurs is given by the same condition as the onset of reverse yielding, namely

$$\begin{aligned}
&f(\zeta_1 k_0) - (k_0 - k)\zeta_1 = -f(\zeta_1 k_0),\\
&\text{i.e.}\quad \frac{\zeta_1}{f(k_0\zeta_1)} = \left(\frac{2}{k_0 - k}\right).
\end{aligned} \tag{A.23}$$

For the regions $0 < \zeta < \zeta_1$ we have elastic unloading as before, but for $\zeta_1 < \zeta < 1$ the original plastic stress must be removed and the new, continuing, work-hardening deformation allowed for. The strain for this is

$$\varepsilon = \zeta(2k_0 - k) - 2f(k_0\zeta), \tag{A.24}$$

and the final result is

$$\begin{aligned}
m_{iv} = {} & m_0 - 2\int_0^{\zeta_1} (k_0 - k)\zeta^2\cdot\,\mathrm{d}\zeta - 2\int_{\zeta_1}^{1} f(k_0\zeta)\zeta\cdot\,\mathrm{d}\zeta - 2\int_{\zeta_1}^{1} f[\zeta(2k_0 - k)\\
&-2f(k_0\zeta)]\zeta\cdot\,\mathrm{d}\zeta.
\end{aligned} \tag{A.25}$$

Now, from the above m–k relationships for the four regions, the general forms for the required areas may be written as

$$G_{db} = \frac{A_1}{b} = G^e_{\max}\left[\int_0^1 m_i \, dk + \int_1^{k_0} m_{ii} \, dk - \tfrac{3}{4}m_0^2 + \tfrac{1}{3}\left[2f(k_0) - \tfrac{3}{2}m_0\right]^2 - \int_0^{k_1} m_{iv} \, dk\right].$$

Hence, we have:

$$\frac{G_{db}}{G^e_{\max}} = \tfrac{1}{3} + \tfrac{4}{3}f^2(k_0) - m_0 f(k_0) + \int_1^{k_0} m_{ii} \, dk - \int_0^{k_1} m_{iv} \, dk. \tag{A.26}$$

And for area A_2 we have

$$\frac{A_2}{b} = G^e_{\max}\left[m_0 k_0 - \tfrac{3}{4}m_0^2 + \tfrac{1}{3}[2f(k_0) - \tfrac{3}{2}m_0]^2 - \int_0^{k_1} m_{iv} \, dk\right].$$

Hence, we have:

$$\frac{G_a^{\infty E}}{G^e_{\max}} = \frac{(1 - \cos\theta)}{[1 - \cos(\theta - \theta_0)]} \cdot \left[m_0 k_0 + \tfrac{4}{3}f^2(k_0) - 2m_0 f(k_0) - \int_0^{k_1} m_{iv} \, dk\right]. \tag{A.27}$$

Thus, the various possible types of deformation of the peeling arm upon being loaded and unloaded may be described by using (A.26) and (A.27) with the appropriate expressions for the values of m $(= m_0)$, m_{ii} and m_{iv} as required, and as defined above. Hence, the three cases of importance during a peel test may be mathematically described. These cases are:

(a) when the bending of the peeling arm, during both the initial loading process (i.e. at the peel front) and the bending of the peeling arm, during both the initial loading process (i.e. at the peel front) and the subsequent straightening and unloading process (i.e. which occurs in the now-debonded peel arm away from the peel front) only involves elastic deformation;
(b) when the initial bending of the peeling arm involves plastic deformation but the unloading and straightening of the arm only involves elastic deformation; and
(c) when the loading and unloading of the peeling arm both involve plastic deformation.

The equations derived from (A.26) and (A.27) for these three cases are given by (9) to (14).

It should be noted that Kim and Aravas [19] discuss these results for a power-law work hardening material, where:

$$f = \left[\frac{\varepsilon}{\varepsilon_y}\right]^N, \quad \frac{\varepsilon}{\varepsilon_y} > 1. \tag{A.28}$$

However, this leads to rather intractable integrals. But, if a bilinear work-hardening model is used instead, where

$$f = (1 - \alpha) + \alpha\left(\frac{\varepsilon}{\varepsilon_y}\right), \tag{A.29}$$

then we may readily evaluate m_{iv} and, hence, obtain (13) and (14) which describe the most important case of when the loading and unloading of the peeling arm both involve plastic deformation.

Appendix B

```
/*          The Peel Test Analysis (Ver 2)                    */
/*   This program uses bi-linear work hardening model         */
/*   to compute the bending dissipation in the peel arm       */

/*       Ga  :adhesive fracture energy                        */
/*       Gdb  :energy dissipated in bending                   */
/*       Geba:fracture energy of elastic bending              */
/*       GinfE:fracture energy assuming inf. rigid arm        */
/*       pbgh:P*B/Gemax                                       */

# include <stdio.h>
# include <conio.h>
# include <math.h>
# define maxi 3000                          /* the max. interation */
# define deltheta0 0.0005                   /* the increment of theta0 */
int i, j, jj;
float alpha, E, ey, theta, theta0, critheta0, h, GinfE, k;
float miderror, begerror, oldtheta0, oldk;
main( )
{                                                    /*BEGIN MAIN*/
        int error_msg;
        float Ga, Gemax, Geba, Gdb, pbgh, error;
        void input_consts( );
        void input_vars( );
        float compute_f2( );
        int check_error(float);
        float compute_f1( );
        float compute_Geba( );
        clrscr( );
        input_consts( );
        for(;;)                                      /*BEGIN ITERATION*/
{
        input_vars( );
        Gemax=E*ey*ey*h/2.0;
        GinfE / =Gemax;                              /* normalising the GinfE */
                                                     /* BEGIN COMPUTING */
        i=0;      j=5;
        theta0=0.005;
        critheta0= 2.*((1.-alpha)/(1.- 2.*alpha))*4.*ey/3.;
        for(;;)                                  /*BEGIN NUMERICAL ITERATION*/
{
        error=compute_f2( ) - GinfE*(1.0-cos(theta-theta0))/ (1.0-cos(theta));
        error_msg=check_error(error);
        if(error_msg !=0) break;
        theta0+ =deltheta0;
        i++;
}                                                /*END NUMERICAL ITERATION*/
```

```
        if(error_msg==1 or error_msg==3)
  {     Gdb=compute_f1( );
        pbgh=GinfE/(1.-cos(theta));
        Geba=compute_Geba(pbgh);
        Ga=Geba−Gdb;
                                                        /*output to screen*/
        printf("\nThe value of Ga (J/m^ 2) = %10.3f", Ga*Gemax);
        printf("\nThe root angle (deg)= %10.3f", theta0*180./3.141593);
        printf("\nThe Geba values (J/m^ 2)= %10.3f", Geba*Gemax);
  }                                                     /*END COMPUTING*/

        printf("\n\nContinue?(y/n)");
        if(getche( ) −− 'n' || getch( ) == 'N') break;

}       getch( );                                       /*END ITERATION*/
}                                                       /*END MAIN*/

        void input_consts( )                            /*Input constants*/
{
        printf("\n\n\n\n");
        printf("input the value of alpha : ");
        scanf("%f", &alpha);

        printf("\ninput the yield strain : ");
        scanf("%f", &ey);

        printf("\ninput the value of E (MPa) : ");
        scanf("%f", &E);
}

        void input_vars( )                      /*Input variables*/
{
        printf("\ninput the thickness (micron) : ");
        scanf("%f", &h);

        printf("\ninput the peel angle (deg) : ");
        scanf("%f", %f", &theta);
        theta * =3.141593/180.;

        printf("\nInput the value of GinfE (J/m^ 2) : ");
        scanf("%f", &GinfE);
        return;
}
        float compute_f2( )
{
        float f2;
        k=3.0*theta0/4./ey;
        if(theta0 <critheta0)           /*plastic loading*/
        {
                f2=k*k/3.0;
                jj=i;
```

```
        if(theta0>critheta0)      /*unloading*/
        {
                j=i-jj;
                f2=alpha*(1.+4.*(1.-alpha)*(1.- alpha))/3.*k*k;
                f2+ =2.*(1.-alpha)*(1.-alpha)*(1. -2.*alpha)*k;
                f2+ =8./k*pow((1.-alpha),4)/(1.-alpha* 2.)/3.;
                f2 + = -4.0*pow(1.-alpha, 3);
        }
        return(f2);
}
        int check_error(float error)          /*checking the results*/
{       float tol=0.00005;
        if(fabs(error) <tol & i>5)
        {
        printf("\nStop 1 : OK, but solutions can be improved by reducing the error tol");
        return(1);
        }

          else
        if(i>maxi)
        {printf("\nStop 2:exceeding the max. no interation (maxi)"); return(2);}
         else
        if(fabs(miderror)<fabs(begerror) & fabs(miderror)< fabs(error) & j>4 & i>5)
        {
                k=oldk;
        theta0=oldtheta0;
        printf("\nStop 3 : successful!");
        return(3);
        }
         else
        if(theta0>theta){printf("\nStop 4 : theta0 >theta-no solution"); return(4);}

        oldtheta0=theta0;                     /*store old values*/
        oldk=k;
        begerror=miderror;
        miderror=error;                       /*store old values*/
        return(0);
}

        float compute_f1()                    /*compute & return f1*/
{
        float f1;
        if(theta0<critheta0)
  {
        f1=(1.-alpha)*(1.*k*k/3.+2.*(1.-alpha)/k/3.-1.);
```

```
        else
  {
        f1=4.*alpha*(1.−alpha)*(1.-alpha)*k*k/3.0
            +2.*(1.−alpha)*(1.−alpha)*(1.−2.* alpha)*k
            +2.*(1.−alpha)*(4.*pow((1.−alpha),3.)+ 1.)/k/3/(1.−2.*alpha)
            −(1.−alpha)*(4.*(1.−alpha)*(1.−alpha)+ 1.);
        return(f1);
  }
}

        float compute_Geba(float pbgh)              /*compute & return Geba*/
{
        if(ey*pbgh/2.<1.0
        return(GinfE+ey*ey*pbgh*pbgh/4.);
        else
        return(GinfE+(ey*pbgh*ey*pbgh/4.+(1.−ey* pbgh))/alpha);
}
```

Acknowledgements. The authors would like to acknowledge the support of Tetra Pak, Romont, Switzerland, and in particular the encouragement and assistance from Dr. Anne Roulin.

References

1. D.W. Aubrey, G.N. Welding and T. Wong, *Journal of Applied Polymer Science* 13 (1969) 2193–2207.
2. D.W. Aubrey, T.A. Jackson and J.D. Smith, *Journal of the Institute of the Rubber Industry* 3 (1969) 265–269.
3. A.N. Gent and R.P. Petrich, *Proceedings Royal Society* A310 (1969) 433–448.
4. D.H. Kaelble, *Journal of Adhesion* 1 (1969) 102–123.
5. Ibid, 124–135.
6. A.N. Gent and A.J. Kinloch, *Journal of Polymer Science, Polymer Physics* 9 (1971) 659–668.
7. P.B. Lindley, *Journal of the Institute of the Rubber Industry* 5 (1969) 243–249.
8. E.H. Andrews and A.J. Kinloch, *Proceedings Royal Society* A332 (1973) 385–399.
9. Ibid, 410–414.
10. K. Kendall, *Journal of Adhesion* 5 (1969) 105–117.
11. A.N. Gent and G.R. Hamed, *Journal of Adhesion* 1 (1975) 91–95.
12. A. Ahagon and A.N. Gent, *Journal of Polymer Science, Polymer Physics* 13 (1975) 1285–1300.
13. A.N. Gent and G.R. Hamed, *Polymer Engineering Science* 17 (1977) 462–466.
14. T. Igarashi, *Rubber Chemistry and Technology* 49 (1975) 1200–1205.
15. A. Ahagon, A.N. Gent, H.J. Kim and Y. Kumagi, *Rubber Chemistry and Technology* 48 (1975) 896–901.
16. A.N. Gent and G.R. Hamed, *Journal of Applied Polymer Science* 21 (1977) 2817–2831.
17. F. Yamamoto, S. Yamakawa and S. Tsuru, *Journal of Polymer Science, Polymer Physics* 18 (1980) 1847–1851.
18. A.N. Gent and S.Y. Kaang, *Journal of Adhesion* 24 (1987) 173–181.
19. K.S. Kim and N. Aravas, *International Journal of Solids and Structures* 24 (1988) 417–435.
20. J. Kim, K.S. Kim and Y.H. Kim, *Journal of Adhesion Science Technology* 3 (1989) 175–187.
21. K.S. Kim and J. Kim, *Transactions ASME* 110 (1988) 266–273.
22. N. Aravas, K.S. Kim and M.J. Loukis, *Materials Science and Engineering* A107 (1989) 159–168.
23. A.N. Gent and C.W. Lin, *Journal of Adhesion* 30 (1989) 1–11.
24. M.D. Thouless and H.M. Jensen, *Journal of Adhesion* 38 (1992) 185–197.
25. J.G. Williams, *Journal of Adhesion* 41 (1993) 225–239.
26. A.J. Kinloch, *Adhesion and Adhesives: Science and Technology*, Chapman and Hall (1987).
27. C.C. Lau, A.J. Kinloch and J.G. Williams, *Proceedings Adhesion Society* Williamsburg, USA (1993).
28. M. Charalambides, A.J. Kinloch, Y. Wang, and J.G. Williams, *International Journal of Fracture* 54 (1992) 269–291.
29. M.F. Kanninen, *International Journal of Fracture* 10 (1974) 415–430.
30. S. Hashemi, A.J. Kinloch and J.G. Williams, *Proceedings Royal Society* A427 (1990) 173–199.
31. A.J. Kinloch and M.L. Yuen, *Journal of Materials Science* 24 (1989) 2183–2190.
32. C.C. Lau, Ph.D. thesis, University of London, London (1993).